Buckling instabilities in periodic composite polymeric materials†

Srikanth Singamaneni*[a] and Vladimir V. Tsukruk*[b]

Received 13th May 2010, Accepted 1st August 2010
DOI: 10.1039/c0sm00374c

Although buckling instabilities in elastic solids have been known for a long time, high interest in this phenomenon is relatively recent. The current and prospective applications in flexible electronics, materials with tunable surface properties (adhesion and wettability), responsive photonic and phononic structures, and reinforced nanocomposites led to a surge in the interest in buckling instabilities. In fact, some of the applications, such as flexible electronics and metrology, have advanced at a tremendous pace only within the past few years. In this review, we discuss some of the most recent progress in the fundamental understanding of buckling instabilities in periodic multi-component polymer materials and porous polymer structures. We also discuss how the buckling can be localized to predetermined regions and hence form periodic instability patterns. Finally, we present several recent examples where buckling instabilities have been employed as a patterning tool to realize complex surface arrays of various materials.

1. Introduction

Mechanical instabilities under high external and internal mechanical stresses are universal phenomena observed at all length scales in a wide range of materials in both natural and man-made systems. Of the various types of instabilities—wrinkling, fingering, snap-through, folding and Rayleigh instabilities to name a few—buckling is the most commonplace in elastic polymeric solids. Reduction in the elastic energy due to out of plane periodic bending caused by either elastic compression or stretching of materials manifests itself in a wide range of everyday phenomena such as wrinkling of the skin, textured cream on milk, and the edges of leaves.

[a]*Current address: Department of Mechanical Engineering and Materials Science, Washington University, St Louis, MO, 63130, USA. E-mail: singamaneni@wustl.edu*
[b]*School of Materials Science and Engineering, Georgia Institute of Technology, Atlanta, GA, 30332, USA. E-mail: vladimir@mse.gatech.edu*
† This paper is part of a *Soft Matter* themed issue on The Physics of Buckling. Guest editor: Alfred Crosby.

Srikanth Singamaneni

Srikanth Singamaneni received his MS degree in Electrical Engineering from Western Michigan University in 2004, his PhD in Polymer Materials Science and Engineering at Georgia Institute of Technology in 2009, and he is currently an assistant professor in the Department of Mechanical Engineering and Materials Science, Washington University in St Louis. He has co-authored nearly 50 refereed articles in archival journals and made numerous presentations at national conferences. He is a recipient of the MRS graduate student gold award Fall 2008 and Best-Poster Award at the Materials Research Society National Meeting, Spring 2007. His current scientific interests include chemical and biological sensors based on nanomaterials and confinement effects in polymers and polymer nanocomposites.

Vladimir V. Tsukruk

Vladimir V. Tsukruk received his MS degree in Physics in 1978 from the National University of Ukraine, PhD and DSc in Chemistry in 1983 and 1988 from the National Academy of Sciences of Ukraine, and was a post-doc at U. Marburg, TU Darmstadt, and U. Akron. Currently, he is a Professor at the School of Materials Science and Engineering and a Co-Director of BIONIC Center, Georgia Institute of Technology. He has co-authored around 300 refereed articles in archival journals, 20 invited reviews and four books. His research activities in the fields of surfaces/interfaces, molecular assemblies, hybrid and bioinspired nanomaterials are highlighted by The Humboldt Research Award (2009), NSF Special Creativity Award (2006), NSF Young Investigator Award (1994), and Best Young Investigator Research Prize in Ukraine (1985) among others. He serves on the editorial advisory boards of five professional journals including Langmuir, Polymer, ACS Appl. Mater. Interfaces *and is a Fellow of American Physical Society.*

From a historical perspective, the irreversible damage of the sandwich panels employed as the primary structural components in the aircrafts used during World War II made buckling an important and technologically relevant phenomenon as was pointed in recent review.[1] Ever since, there has been continued effort to further our understanding of this ubiquitous phenomenon at multiple length scales, complex structural systems (free standing films and floating films) and material systems. The simplest and arguably the most studied system is stiff skin layer attached to a thick elastic foundation, much like the human skin (thin and stiff epidermis layer on a thick and soft dermis). The compressive force on the rigidly attached skin layer is given by:

$$F = E_s\left[\left(\frac{\pi}{\lambda}\right)^2 \frac{wh^3}{3\left(1-\upsilon_s^2\right)} + \frac{\lambda}{4\pi}\frac{E_f w}{\left(1-\upsilon_f^2\right)E_s}\right] \quad (1)$$

where h and w are the thickness and width of the skin layer, λ is the sinusoidal deflection profile, E_s, υ_s and E_f, υ_f are the elastic moduli and the Poisson's ratio of the skin and foundation layers. The critical strain and the critical buckling wavelength can be obtained based on the above consideration. For a more detailed discussion of the mechanistic aspects and analytical analysis the readers are referred elsewhere.[2–6] More recently, a different approach based on the balance between the bending energy of the skin and the stretching energy of the foundation has been put forward by Cerda and Mahadevan. The readers are referred to original articles and a recent review for the details.[1,7,8]

Buckling instabilities in metals, ceramic and polymeric thin films have received intense attention in the last years. Buckling behavior has been extensively investigated in homogenous freely suspended and substrate supported[9–13] or floating thin films[14] of metals, polymers, and various nanostructures (polymeric[15] and inorganic nanowires,[16,17] carbon nanotubes[18]). Buckling instabilities have been demonstrated to be valuable in controlling adhesion,[19,20] enabling flexible electronics,[21,22] providing means for micro- and nanopatterning[23] and optical microdevices based upon micrograting.[24] Complex and highly localized buckling instability patterns have been created, observed and characterized in thin and ultrathin metal and polymer films by various techniques such as patterning metal nanoparticles in polymer films, local oxidation of the elastomeric substrate and surfaces.[9,25] Some of these approaches and corresponding results will be discussed in this review.

However, the main focus of this brief review is on complex and non-traditional buckling phenomena in periodic composite polymeric structures of different complexities ranging from ultrathin polymer films to two- and three-dimensional porous structures with many illustrations coming from the authors' own recent studies of this class of polymeric materials. The readers are referred to several excellent reviews and feature articles covering various aspects of conventional buckling behavior in homogenous polymeric materials.[1,26,27]

2. Buckling instabilities in composite thin films

Uniform thin films are a subject of numerous studies. However, only relatively recently Stafford *et al.* have introduced strain-induced elastic buckling instability for mechanical measurements (SIEBIMM) as a novel metrology technique for measuring the mechanical properties of uniform thin films.[28] The technique, which was immediately embraced for polymer thin film studies, involves a thin, stiff polymer layer firmly bound to a compliant substrate, which is subjected to a compressive stress to induce buckling instabilities. The periodicity of the uniform buckling pattern is given by:

$$\lambda = 2\pi t\left[\frac{\left(1-\upsilon_s^2\right)E_f}{3\left(1-\upsilon_f^2\right)E_s}\right]^{1/3} \quad (2)$$

where λ is the wavelength of the periodic buckling pattern, E_f and υ_f are the elastic modulus and Poisson's ratio of the film, and E_s and υ_s are the elastic modulus and Poisson's ratio of the compliant substrate, and t is the thickness of the film.

In this pioneering work, Stafford *et al.* employed thin polystyrene (PS) deposited on elastomeric polydimethylsiloxane (PDMS) to demonstrate the novel metrology technique. Fig. 1a shows the design with the PDMS substrate and the thin polystyrene film deposited on top. Gentle lateral compression of the compliant PDMS leads to the compression of the PS film, which buckles at a certain threshold stress and generates the periodic wrinkles on the film surface, as shown in the AFM image (Fig. 1b). The technique has been extensively employed for measuring the modulus of thin polymer films either deposited, assembled, or transferred on complaint substrates with the most popular being PDMS due to its high compliance, easy surface modification, and wide range of achievable strains and stresses. The thin film buckling phenomenon has been exploited as a novel metrology technique for measuring elastic moduli of nanoscale polymeric films, composite nanomembranes, as well as 1D and 2D nanostructures, for which conventional mechanical testing approaches cannot be readily applied.[14,16,18]

The technique has been extended to probing the mechanical properties of ultrathin films of a variety of synthetic polymers as well as biopolymers such as silk fibroin materials. For instance, Jiang *et al.* have measured the mechanical properties of ultrathin silk films formed by spin coating and spin-assisted layer by layer assembly.[29] Fig. 2 shows the buckling patterns in the silk films obtained with layer by layer (LbL) assembly and treated with methanol or water on PDMS under compressive stress. From the buckling patterns, the elastic modulus of the methanol treated LbL silk film (6.5 GPa) with thickness below 100 nm was found to be much higher than that of the water treated film (3.4 GPa), which in turn exhibited higher elastic modulus as compared to

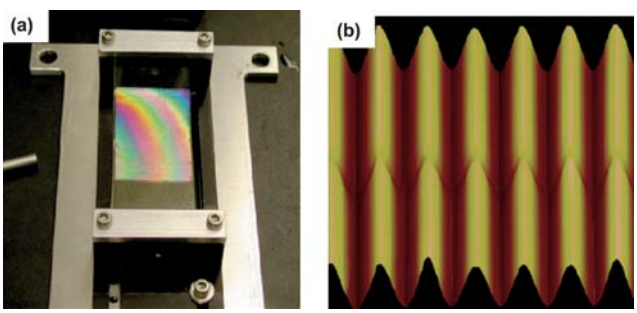

Fig. 1 (a) A typical buckling setup with a thin PS film deposited on PDMS substrate. (b) AFM image showing the uniform sinusoidal buckling of this film under compressive stress. Reprinted from ref. 28.

the submicron thick cast silk film (2.8 GPa) also studied in this work (Fig. 2).

As mentioned in the Introduction, buckling instabilities have been extensively explored in thin rigid skins on compliant substrates. However, they remain relatively underexplored and elusive in ultrathin, nanoscale gels firmly tethered to rigid surfaces, which impose strong restrictive boundary conditions. Recently, Singamaneni *et al.* have demonstrated uniform folding of an ultrathin (<100 nm) crosslinked poly-2-vinyl pyridine film when swollen in an acidic solution.[30,31] In these highly compliant polymeric systems, uniform sinusoidal buckles are insufficient to relieve the swelling-induced stresses, causing the stress to localize into pinched buckles, which finally fold. The characteristic dimensions (length and width) of the folds scale with the thickness of the film and were related to the buckling period of the *de novo* patterns formed in the initial stages of swelling. The large volumetric expansion of the swollen ultrathin gel forces the system to explore modes beyond simple linear elastic buckling and into an out-of-plane deformation mode.

The SIEBIMM technique has been extended to various composite polymer films, which are inhomogeneous in either vertical or lateral directions. Nolte *et al.* have extended the metrology technique to vertically stratified bilayered structures.[32] The mechanical contribution of individual layers was suggested to be deconvoluted from the experimental data for the composite films to deduce a Young's modulus of the desired layer. The authors investigated the elastic modulus of polyelectrolyte membrane (PEM) assembled on a thin PS film transferred onto a PDMS substrate. Compression of the PS/PEM structure resulted in the buckling of the composite structure with different periodicities. A simple analytical relation was derived for calculating the elastic modulus of the PEM from these data as:

$$\bar{E}_{\mathrm{PEM}} = \frac{\frac{\bar{E}_{\mathrm{eff}}}{4} - \bar{E}_{\mathrm{PS}}\left[\left(\phi_{\mathrm{PS}} - \frac{\kappa}{2}\right)^3 + \left(\frac{\kappa}{2}\right)^3\right]}{\left(1 - \frac{\kappa}{2}\right)^3 - \left(\phi_{\mathrm{PS}} - \frac{\kappa}{2}\right)^3} \quad (3)$$

where the overbars indicate the reduced elastic modulus given by $E/(1 - \upsilon^2)$, $\bar{E}_{\mathrm{PEM}}$, $\bar{E}_{\mathrm{PS}}$ and $\bar{E}_{\mathrm{eff}}$ are the reduced elastic moduli of the PEM, the PS, and the PS and PEM film, respectively, and ϕ_{PS} is the thickness fraction of the PS film. The authors experimentally verified the validity of this two-layer buckling model by comparing the elastic modulus of PEM films in the PEM/PS composite structure with that obtained for the PEM film deposited directly on the PDMS substrate.

Buckling has been extensively applied for the determination of the modulus of ultrathin polymer films filled with inorganic nanostructures (nanoparticles and nanowires).[33–35] For example, Jiang *et al.* have employed SIEBIMM to obtain the elastic properties of PEM films filled with patterned nanoparticles with 10 μm periodicity (see Fig. 3a).[34] Upon compression, the composite film exhibited a complex zigzag buckling pattern with two distinct buckling periodicities in the areas with and without gold nanoparticles, as shown in Fig. 3b. The estimation of the elastic properties of two different regions using eqn (2) resulted in an elastic modulus of 3.0 GPa for the regions with nanoparticles while the elastic modulus for the polymeric regions was found to be much lower at 1.6 GPa. The values obtained by the buckling technique were found to be in good agreement with independently measured elastic moduli of the uniform LbL films.[36,37] The buckling patterns observed for patterned films in this work enable "one-shot" evaluation of the elastic moduli of two compositionally different regions (with and without gold nanoparticles).

In another study, Jiang *et al.* observed dynamic buckling in freely suspended gold nanoparticle filled PEMs which were deposited onto a patterned silicon substrate and deformed by variable pressure (Fig. 4).[38] The membranes suspended across cavities exhibited transformations from concave to convex shapes due to the thermally driven expansion and contraction of the air sealed in the cavities. The shape transformation of the freely suspended membranes was accompanied with

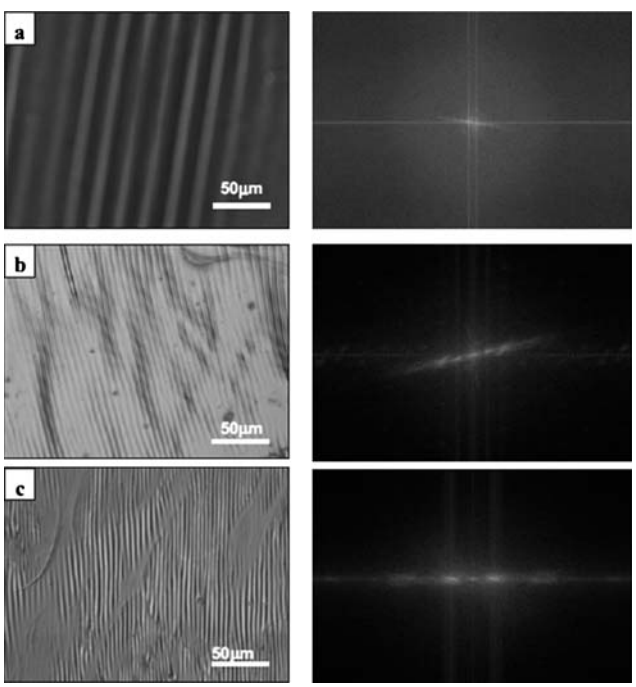

Fig. 2 Optical images of the buckling patterns and the corresponding 2D fast Fourier transforms (FFTs) of silk films fabricated by (a) casting, (b) LbL assembly with water treatment, and (c) LbL assembly with methanol treatment. Reprinted from ref. 29.

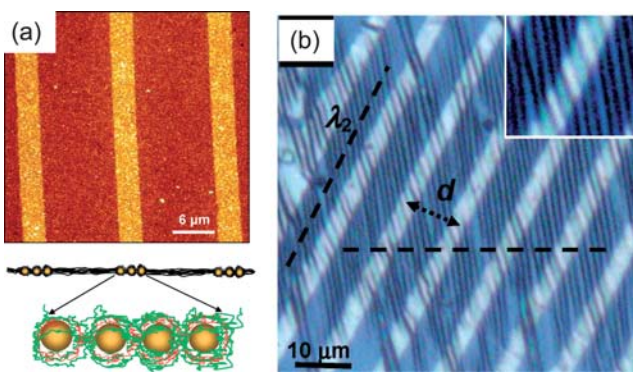

Fig. 3 (a) AFM image showing the patterned arrays of AuNP in the LbL film and the schematic of the nanoparticles incorporated within the LbL films. (b) Optical image showing the buckling of the film in both the regions with and without nanoparticles with different periodicities (inset shows the zigzag buckling at the interface of the two regions). Reprinted from ref. 34.

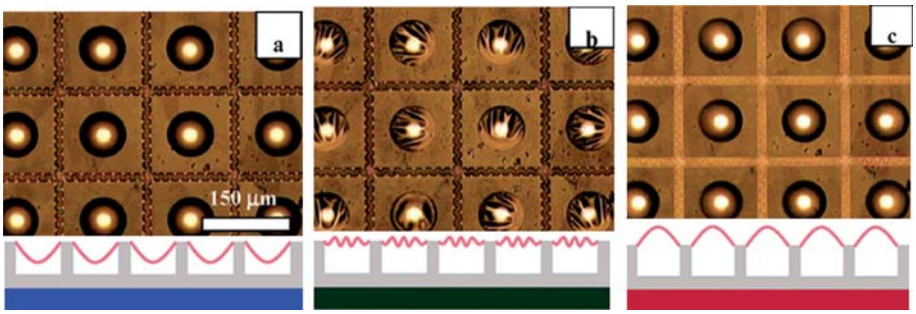

Fig. 4 Optical micrographs of nanocomposite PEM film suspended over microfabricated cavities showing the (a) convex (low temperature), (b) flat, and (c) concave (at elevated temperature) states of the films with variations in temperature. Buckling of the nanomembrane during the transformation (flat state) and the worm-like buckles in the trenches can be clearly identified in the optical images. Reprinted from ref. 38.

distinguished buckling patterns separating two uniform states (concave and convex), as can be seen on circular openings in Fig. 4. Furthermore, the buckling instability of the membrane freely suspended across the cylindrical cavity was accompanied by the formation of the wormlike instability pattern along rectangular trenches (Fig. 4). These patterns were found to be completely reversible and, similar to snap-through membrane behavior, were associated with localized surface instabilities caused by fast stress relief during the transition between two stable deformational states.[39] These rapid buckling-induced transitions suggest the possible application of the phenomenon for sensing and actuation.

There are numerous theoretical studies which have recognized buckling as a possible sensing mechanism that is incredibly sensitive, but has a very small sensing range due to the discrete nature of buckling.[40,41] Sensitivity could be an order of magnitude higher than that of conventional linear transduction, such as bending microcantilevers.[42] Much of the enhanced response can be attributed to stress that builds prior to the critical buckling point, which acts to amplify the snap-type response. In a related study, McConney *et al.* have exploited the buckling instabilities in freely suspended composite nanomembranes as a highly sensitive platform for sensing minor environmental changes.[43] The authors demonstrated a thermal sensitivity of 10 mK by monitoring the relative optical signal from the buckling transformation of freely suspended membranes. The demonstration is quite impressive considering the extremely small footprint of these sensors (~15 μm) which severely impairs sensing characteristics of conventional membrane sensors.

There are numerous examples where buckling has been employed to measure the elastic properties of ultrathin composite films—a highly non-trivial task for traditional testing methods. Gunawidjaja *et al.* have employed the SIEBIMM technique to probe the elastic modulus of LbL films with encapsulated silver nanowires.[44,45] It was found that the elastic modulus of these ultrathin films (<100 nm) increased with the silver nanowire volume fraction from 1.7 GPa (0%) to 5.7 GPa (22.5%). They compared the values obtained by buckling to values obtained from an independent technique, which involves bulging the same films in a freely suspended state under hydrostatic pressure. The values obtained from both the techniques were found to be fairly similar with buckling, yielding slightly higher values compared to the bulging method. Furthermore, buckling was found to be extremely close to the theoretically calculated values for oriented reinforcing nanostructures. One of the important differences between both of the techniques is that the buckling method involves compression of the film while bulging involves tensile forces on the films. This fundamental difference in the loading mode might contribute to the systematic differences in the elastic modulus values obtained with both the techniques for many polymeric materials.

In a related study, Gunawidjaja *et al.* aligned the silver nanowires within the LbL membranes using the Langmuir–Blodgett approach.[46] When the films were compressed in the direction parallel to the silver nanowires, uniform buckling was observed over large areas of the films, while, on the other hand, compression in the perpendicular direction resulted in sporadic buckling localized at the silver nanowires. Applying the SIEBIMM analysis, the modulus was found to be 0.7 GPa in the direction perpendicular to the filler while the same was found to be 3.8 GPa along the nanowire orientation. Furthermore, the buckling of the silver nanowires was analyzed using one-dimensional Euler instability and the modulus of the silver nanowire was calculated to be 118 GPa—close to the 124 GPa elastic modulus for the (100) direction of bulk silver.

Whereas buckling of thin, stiff films rigidly bound to compliant substrates is common, Lee and Hendricks have demonstrated that this phenomenon can be suppressed in PEMs filled with silica nanoparticles.[47] The PEMs readily buckled for low volume fractions of silica particles in the polymer films (1 layer of 50 nm silica particles in 20 polymer bilayers). However, when the volume fraction of the silica layers was increased three-fold, the films did not exhibit buckling under external stresses. This is rather surprising considering that the presence of the silica particles enhances the modulus of the polymer films, thus lowering the critical stress required to buckle. The authors speculated that the nanoparticles in the film break up, alleviating the stress and thus preventing the film buckling. However, the exact mechanism of the wrinkle inhibition with nanoparticles remains elusive.

3. Buckling instabilities in periodic porous structures

Lightweight organized porous structures composed of beams and nodes (joints) are designed to optimally bear anticipated loads.[48] Such structures possess excellent strength- and stiffness-to-weight ratios and are very familiar to civil and mechanical

engineers. Recently, microscopic analogs of these structures have been extensively investigated with envisioned applications as diverse as lightweight armors to tissue engineering scaffolds.[49–52] These porous periodic microstructures display increased compressibility moduli of up to 70% due to the increased connectivity. From a structural applications standpoint, the design of materials for ultimate mechanical properties should provide optimal loading conditions such that beams are under compression or tension while avoiding bending.[53] However, the structural failure in the form of local buckling might impair their performance.

Thus, Mullin and coworkers have investigated the mechanical instabilities in millimetre scale periodic porous structures subjected to uniaxial strain.[54] Thin sheets (~10 mm) with square and rectangular lattices of pores were fabricated using a photoelastic elastomer with the birefringence of the material varied under mechanical strain. The square and rectangular lattice samples were comprised of circular holes and were subjected to uniaxial compressive stress along the (10) direction. In the initial linear elastic regime, the authors have observed a gradual and homogeneous compression of the circular holes, which is replaced by a transformation to a strikingly different pattern of alternating mutually orthogonal ellipses above a nominal strain of 0.04. The pattern transformation was found to be the result of compressive loading of the struts which undergo a buckling instability, thereby triggering the transformation. The buckling was found to be completely elastic with the deformed pattern reversing to its original state upon stress removal. The authors noted that the buckling instability observed in these macroscopic structures should persist even at micro- and nanoscales.

Numerical simulation of this deformational behavior was further investigated utilizing nonlinear finite element analysis (FEA). The elastomeric stress–strain behavior was modeled as a nearly incompressible neo-Hookean solid. Two different modeling approaches were adapted in this study. In the first approach, a representative volume element with the appropriate periodic boundary conditions was employed. In the second approach, the full specimen was considered to capture any boundary effects on either constraining (top or bottom surfaces) or triggering (free side surfaces) the transformation. From the numerical modeling and the experimental observations, it was found that the large deformation associated with the pattern transformation is accommodated by the alternate bending of the struts along both (10) and (01) directions and the alternate rotation of the nodes in clockwise and counterclockwise directions along both (10) and (01) directions, as shown in Fig. 5. Furthermore, the stress distribution following the pattern transformation was monitored owing to the birefringence properties of the elastomeric structures. The stress was found to be localized in the struts, in excellent agreement with the FEA modeling predictions (see Fig. 5, right column).

In another study, Triantafyllidis *et al.* have predicted that the onset of failure of two-phase periodic polymer structures under biaxial strain to be a result of local structural instabilities.[55] The onset of failure was considered as the point at which an instability initiates and local deformation occurs in the material. In contrast, the observations of Mullin and coworkers' study suggested that not only the onset, but also further accentuation of the buckling instability and the associated pattern transformation are homogenous over the entire porous structure and the deformation is not constrained to only few cells but can extend to large areas (see below).[54]

As mentioned above, periodic porous structures might act as photonic and phononic structures depending on the scale. Perceivably, the large and dramatic transformation of the pattern in these structures might cause a dramatic change in their relevant physical properties. In fact, Bertoldi and Boyce have demonstrated that the pattern transformation of the periodic porous structures results in opening up of new band gaps in the phononic structures.[56] In the initial linear elastic regime of deformation, the band gaps

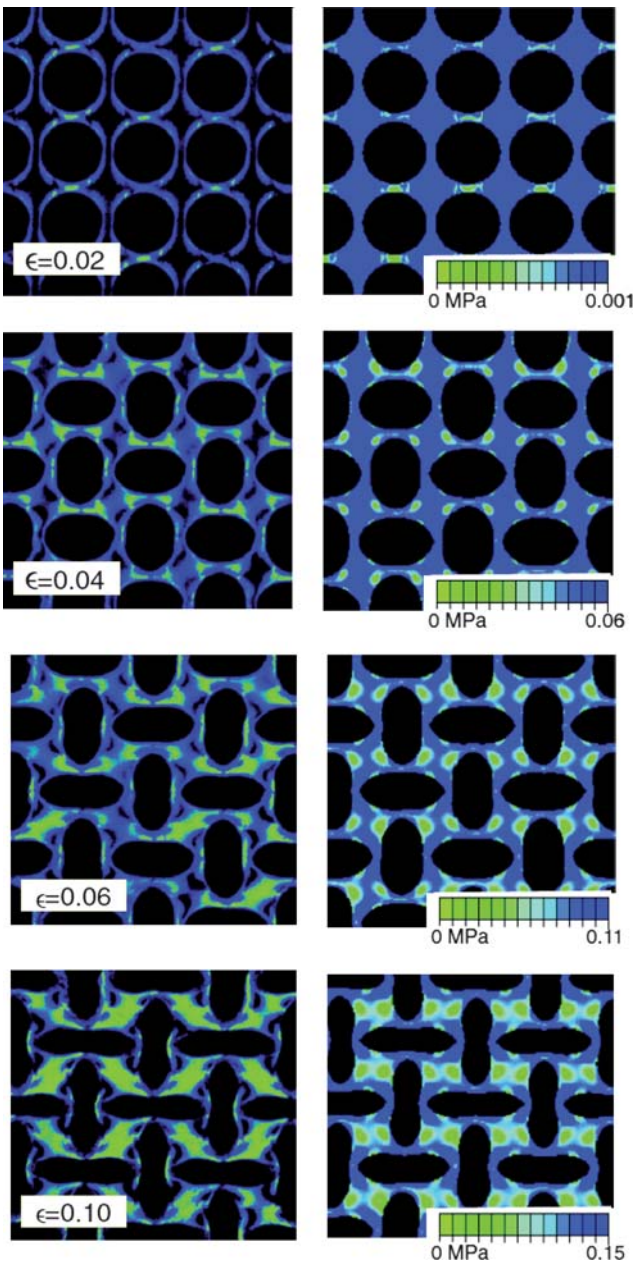

Fig. 5 (left) Experimental and (right) FEA modeling of the porous structures subjected to uniaxial strain exhibiting the pattern transformation beyond the critical strain. The deformation of the structure and the stress distribution can be seen in both the images to be remarkably similar. Reprinted from ref. 54.

were found to evolve in an affine manner. However, above the critical strain, the sudden pattern transformation was found to strongly affect the in-plane phononic band gaps of the porous structures resulting in the closure of existing band gaps and in the opening of new ones. Owing to the elastic nature of the periodic structures employed, the transition in the phononic band gap structure was completely reversible.

In a different study, Bertoldi *et al.* demonstrated that the pattern transformation in the periodic porous structures was accompanied by a negative Poisson's ratio.[57] Fig. 6 shows the corresponding pattern transformation in elastomeric structures subjected to uniaxial compression. It can be clearly observed from the optical images that the structure exhibits compression in the direction perpendicular to the direction of the external uniaxial compressive stress. The critical strain for the onset of the buckling instability in these structures was found to be 0.047. The Poisson's ratio starts to decrease above this point and eventually becomes negative for normal strains in excess of 0.053. The Poisson's ratio as a function of the applied stress estimated from FEA shows excellent agreement with the experimentally observed transition (Fig. 6c).

Pattern transformation in microporous structures

Pattern transformation caused by buckling instabilities in periodic porous structures has been demonstrated at multiple length scales (mm to sub-μm), in a variety of pore geometries and lattice symmetries, and for a wide range of materials. In this section, we will briefly discuss some important recent examples which highlight the scale invariance and versatility of the phenomenon. It is important to note that mechanics of the pattern transformation (such as rotation of the nodes, bending of the struts and substrate constraints) instability holds across multiple length scales (*i.e.* for the macroscopic structures discussed above and microscopic structures that will be discussed below).

Two important challenges that should to be addressed to extend the buckling-related pattern transformation to the micro- and nanoscale are: (i) fabrication of periodic porous structures with well defined order over large areas and (ii) application of uniform mechanical stress to trigger the mechanical instability. Fabrication of such periodic structures was realized by using interference lithography (IL), an elegant fabrication technique that allows the creation of 1D, 2D, and 3D periodic patterns and predetermined highly porous architectures. For instance, in recent study Zhang *et al.* have employed the square array of vertical posts as a master for the fabrication of microporous elastomeric PDMS structure.[58] The structure was comprised of a square array of circular pores with the pore diameter ranging from 350 nm to 2 μm and an aspect ratio (pore depth/diameter) ranging from 2 to 20. Pattern transformation in these structures was triggered by material swelling mediated stress caused by exposing the PDMS microporous structure to toluene. The instability-induced transition was elastic in nature and the structures reversed back to their original state upon the evaporation of toluene. However, fast evaporation of the toluene imposed severe limitations on their full structural characterization.

Overcoming this limitation, Singamaneni *et al.* have investigated the buckling instabilities in different elasto-plastic porous microstructures (square and hexagonal lattice), which were also

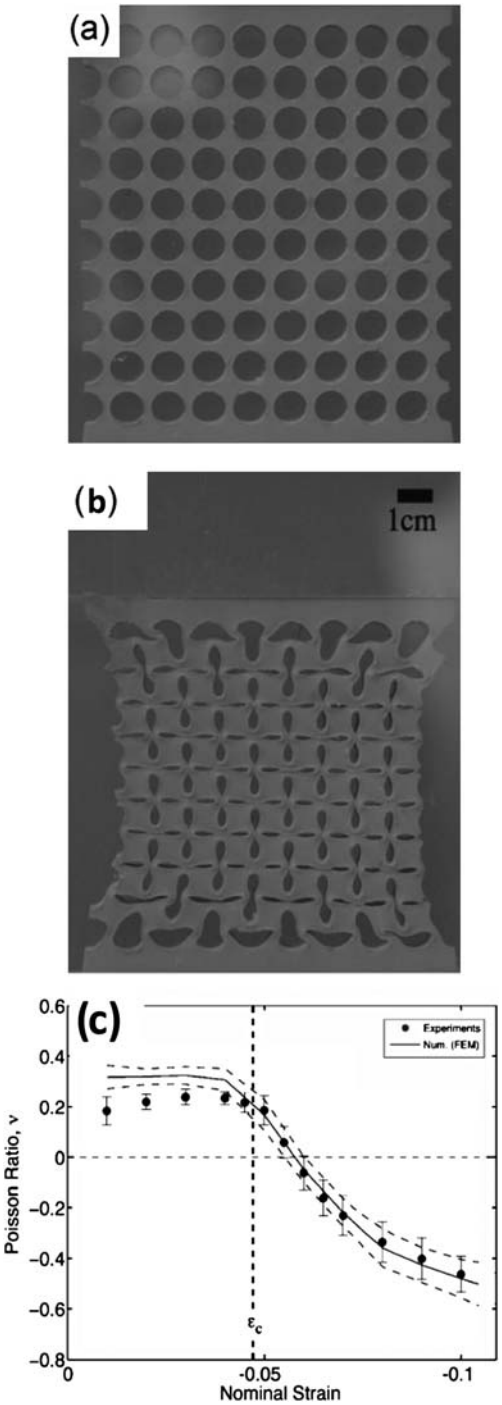

Fig. 6 Optical images of (a) pristine periodic porous structure and (b) the deformed state of the porous structure under uniaxial compression along the perpendicular direction. (c) Experimentally determined and FEA derived Poisson's ratio of the structures at different strains. Reprinted from ref. 57.

fabricated by interference lithography.[59,60] The elasto-plastic nature of the Bisphenol A Novolak epoxy (SU8) enabled the freezing of the buckling instability, providing a better system for understanding the details of the microstructure in transformed structures. The periodicity of the square lattice in this study was

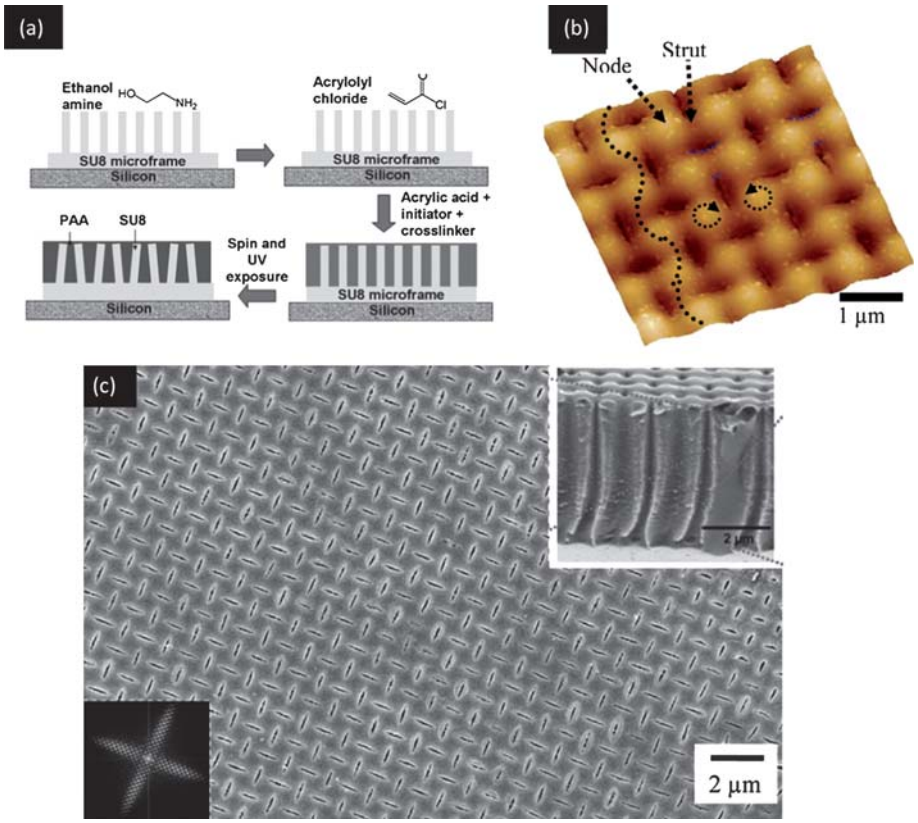

Fig. 7 (a) Schematic showing the infiltration of the acrylic acid (monomer) into the pores followed by photopolymerization to trigger the buckling instabilities in the porous structure. (b) AFM showing the rotation of the nodes and bending of the struts in alternate directions. (c) SEM image showing the uniform pattern transformation over large areas in the periodic porous structure following the polymerization of the acrylic acid in the pores. Reprinted from ref. 59 and 60.

830 nm, the diameter of the cylindrical pores was 380 nm and the porosity was 20%. The corresponding oblique lattice fabricated in a similar manner had a periodicity of 1 μm, a radius of 200 nm and a porosity of 35%. The thickness of the microframe structures was 3 μm, resulting in an aspect ratio of nearly eight.

In order to induce mechanical instabilities in these structures, *in situ* solution photopolymerization of acrylic acid monomer was performed directly in the cylindrical pores (see schematics in Fig. 7a). The slow evaporation of water from inside of the open cylindrical micropores causes the swollen polyacrylic acid (PAA) network grafted to the pore walls to shrink, resulting in high compressive stresses inside pores. These stresses resulted in a dramatic transformation of the periodic circular holes to alternating ellipses in the case of the square lattice and sheared ellipses in the case of the oblique lattice (Fig. 7). Transformed regions were extremely uniform, extending to surface areas up to a few millimetres. The variation of the deformational level through the thickness of the specimen for the square array can be seen in the SEM image of the transformed structure (Fig. 7). Such a vertical gradient is caused by the constraint generated by the substrate on the lateral deformation in the vicinity of the buffer layer.

The AFM image clearly reveals the structural transformation at a microscopic level (Fig. 7b). The pattern transformation can be related to bending of the struts in alternate directions (along (10) and (01) directions) and the rotation of the nodes in clockwise and counterclockwise directions, as indicated on the AFM image. The elasto-plastic nature of the IL material deformation locked in the mechanical instabilities after the release of the external stress with internal stresses dissipated to a great extent, as was confirmed by micromapping with Raman spectroscopy. This observation is in sharp contrast with the reversible instabilities in elastomeric solids, in which the transformed structures exhibit stress concentration in localized, highly deformed elements.

This ability to lock in the transformed pattern of buckling instabilities was exploited to demonstrate a tunable phononic structure by Jang and coworkers.[61] Similar to the method employed for the elastomeric PDMS microporous structures described earlier, the authors have employed swelling induced buckling by exposing the crosslinked bisphenol A Novolak epoxy structures to *N*-methylpyrrolindone (NMP, a good solvent for this polymer). Swelling resulted in the transformation of a hexagonal array of circular pores (diameter of 410 nm) to oval shaped pores and the transformation of an oblique lattice into a herringbone pattern. Following the pattern transformation, the samples were immersed in isopropyl alcohol (a bad solvent for this polymer), which caused the mechanical instability to be locked into the structure owing the fast rise of the glass transition, which limited the mobility of the polymer. Moreover, pattern transformation could be successfully reversed by exposing the transformed structure to NMP vapor, which lowered the glass transition sufficiently to revert the pattern transformation while not inducing swelling to retrigger the buckling instability.

4. Patterned buckling and buckling as a patterning tool

Patterning buckling instabilities

Spatial confinement of mechanical instabilities involves either confining the external stimulus (mechanical stress, solvent and heat) to localized regions of the material system or spatial variation of the properties of material system, which are sensitive to the onset of buckling. In fact, both of these approaches have been widely exploited. Here, we will briefly discuss some recent examples involving complex hierarchical transformed patterns achieved by patterned mechanical instabilities.

Highly localized and complex buckling patterns were demonstrated in ultrathin LbL polymer films filled with patterned arrays of metal nanoparticles.[34] It was suggested that the presence/absence of gold nanoparticles in the different regions of these composite structures would result in different elastic properties, which in turn would affect their buckling behavior, leading to complex buckling of the instability pattern. Indeed, gentle compression (~0.2% strain) of the LbL film along the stripes resulted in immediate appearance of peculiar transversal periodic buckling patterns *strictly* confined to stiffer gold nanoparticle-containing regions with almost none of them extending over to pure-polymeric regions (Fig. 8).

The confinement of the buckilng instabilities to selected areas could be explained by considering the change of the critical strain to trigger buckling of the stiff skin on compliant substrate. As is known, the critical strain for buckling is given by:[62]

$$\varepsilon_c = -\frac{1}{4}\left(\frac{3E_s}{E_f}\right)^{2/3} \quad (4)$$

where E_s and E_f are the elastic moduli of the substrate and film, respectively. From this simple relationship, it is clear that the critical strain is smaller for stiffer films. Thus, the regions reinforced with gold nanoparticles, which are much stiffer compared to the unfilled regions, exhibit lower critical strain and thus exclusively buckle under smaller strain, leaving the purely polymeric regions unbuckled. However, both regions exhibited instabilities at even higher stresses with complex zigzag buckles across the stiff and compliant regions, as was discussed above (Fig. 3).

In another interesting study, Lu and coworkers reported a novel method to spatially control the buckling of the PEM films on flexible substrates.[63] The authors demonstrated regiospecific wrinkling when a three step processing was applied. In this approach, the PDMS substrate was first modified by oxygen plasma followed by the LbL deposition which is in turn followed by embossing using a silicone master. The buckling of the PEMs and the surface relief patterns achieved were governed by the wetting behavior of the PEMs on the PDMS substrates. The authors noted that in the cracked regions, the presence of the unoxidized hydrophobic PDMS surface areas caused the PEMs to de-wet and form the intriguing concentric wrinkle topography confined to specific surface areas.

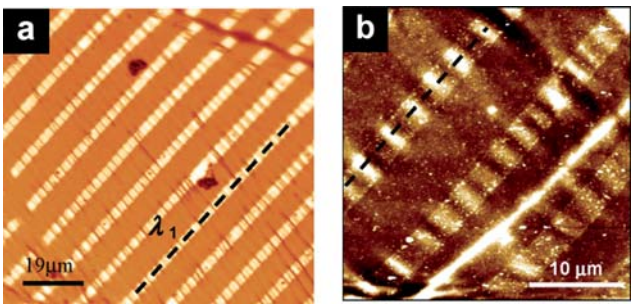

Fig. 8 (a) Optical and (b) AFM images of the buckling patterns localized to the regions in the PEMs filled with Au nanoparticles due to the lower critical strain for buckling of these stiffer regions compared to the unfilled regions. Reprinted from ref. 34.

Localization of the buckling instabilities was also achieved in the case of periodic porous structures with polymerization inside the pores, which was discussed above (Fig. 7a).[60] Localized pattern transformation was spatially confined by periodic mechanical stresses achieved by filling predetermined areas of the porous structure with acrylic acid monomer while preventing the infiltration into the other pores (Fig. 9a). Capillary transfer lithography was employed for selectively depositing a PS pattern with a periodicity of 10 μm for blocking certain porous areas.[64,65] Selective photopolymerization in the exposed areas resulted in localized transformation and a superlattice pattern with periodicity of 10 μm (Fig. 9). The SEM image clearly demonstrates the array of mutually orthogonal elliptical pores (transformed areas) interleaved with the array of circular pores (intact areas) with extremely sharp transition zones between these two regions as discussed below. The transition between the pristine and transformed regions was found to be sharp in the case when the stripe pattern was aligned with the lattice direction of periodic pores. On the other hand, gradual transition between the pristine and transformed regions was observed in the case of slight misalignment between the stripes and the (10) direction of the square lattice.

One important theoretically predicted feature, vertical compression of the structure during pattern transformation, was experimentally verified by the localized pattern transformation.[60] AFM topography and the corresponding cross-sections clearly revealed the compression of the transformed regions along the normal direction as compared to the pristine regions (Fig. 9). In fact, the cross-section analysis reveals that the transformed regions were compressed by about 150 nm (corresponding to 5% strain) in the vertical direction compared to the pristine porous regions. Thus, the patterning of instabilities confirmed that the pore collapse occurs not only in the (x, y) plane of the microstructure but also significantly perturbs the porous structure in z direction.

In a different approach, Zhu *et al.* demonstrated confinement of the pattern transformation in porous PDMS structures by locally modifying the properties (swellability) of the porous PDMS structures.[66] The porous microstructure was exposed to oxygen plasma using a copper TEM grid as a physical mask. The porous microstructures with patterns of oxidized regions were exposed to toluene to induce swelling of selected unoxidized regions and hence pattern transformation. Since the oxidized regions of the PDMS are not swollen in toluene, the pattern transformation was found to be localized only to the masked regions.

Buckling as a patterning tool

Patterning of micro- and nanostructures utilizing uniform buckling patterns was demonstrated by Lu and coworkers.[23]

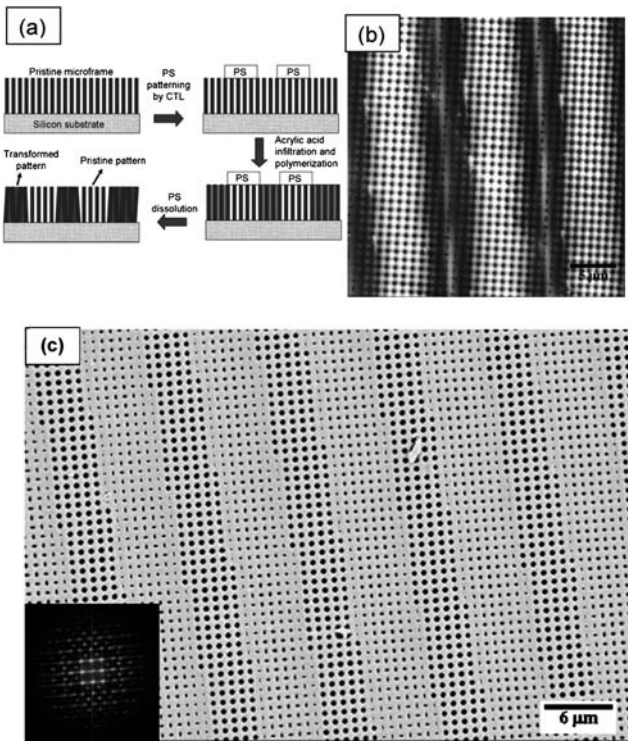

Fig. 9 (a) Schematic showing the localized infiltration of the acrylic acid into selected pores while blocking the other pores followed by polymerization to result in patterned buckling instabilities. (b) AFM and (c) SEM images (large area) showing the arrays of transformed regions interleaved with pristine regions. Reprinted from ref. 60.

They created ordered arrays of colloidal particles on buckled PEM on PDMS using a simple dip coating process. The substrate with a wrinkled surface was dipped into a colloidal suspension with the same orientation of the wrinkle's grooves with withdrawing direction of dipping (Fig. 10a). They have found that successful registry occurs when the features of the template (wavelength and height of the wrinkles) are of the same dimensions. Furthermore, adhesion of particles to the surface needs to overcome weak repulsive forces. Under these conditions, ordered arrays of densely packed particles (down to a single particle row) were obtained with the deposited geometry controlled by the periodicity and height of the buckled surface (Fig. 10b).

In another study from this group, Pretzl *et al.* demonstrated the application of buckling patterns to pattern PEMs and proteins.[67] The authors have replaced the conventional PDMS stamp (negative replica of a microfabricated master) in a microcontact printing technique with PDMS with frozen periodic wrinkles (Fig. 11a). Chemical patterns of polyelectrolytes were formed on a flat surface by gentle mechanical contact of a wrinkled surface inked with the desired chemical species (polyelectrolytes or proteins). The obtained patterns exhibited excellent uniformity with periodicities below 1 μm, which are difficult to achieve with conventional photolithographical microstamping (Fig. 11b and c).

Buckling instabilities in periodic porous structures have also been extensively employed as a versatile patterning tool. In a series of publications, Yang's group has demonstrated a truly remarkable library of nanoparticle patterns that can be achieved using buckling of elastomeric structures.[58,66,68] As discussed earlier, in these studies the buckling-induced pattern transformation in periodic porous PDMS structures was achieved by swelling them in toluene. The periodic porous PDMS substrates with square arrays of pores were swollen using a toluene solution of nanoparticles. The swelling causes the compressive stress and hence pattern transformation, as has been discussed above. However, the presence of nanoparticles in solution results in effective trapping of these nanoparticles in the collapsed pores (Fig. 12).

As a next step, the trapped nanoparticles can be released by pressing the PDMS substrate against a stiff wall and eventually printed onto a desired substrate, resulting in a mutually orthogonal pattern of nanoparticles which follows the transformed pattern (Fig. 12). In further studies, the authors have extended the technique to a much more complex structure by changing the geometry and the symmetry of the initial pores (by stretching the PDMS substrate, for example).[68] Furthermore, in a recent example they have employed the assembled nanoparticles as masters to fabricate a PDMS replica, which in turn was employed to fabricate intricate patterns by imprinting the patterns into a photoresist followed by etching (see schematic Fig. 12a). By controlling the etching time they were able to achieve fine control over the gold nanoparticle patterns on the surface, as depicted in Fig. 12b.

Finally, the topographical features of the buckling-induced transformation patterns in IL structures were replicated in a common glassy polymer such as PS, by using CTL process.[64] The process involves the fabrication of a negative replica (stamp) of the transformed pattern from epoxy-bisphenol structures by using PDMS substrates. The stamp is then used again to replicate the transformed pattern in PS. The resulting polystyrene replica with mutually orthogonal ellipses resembled those in the transformed master.

4. Conclusions

In this review, we summarized the recent efforts in advancing the versatility and complexity of buckling instabilities in multicomponent systems such as ultrathin multilayered polymer films, nanoparticle filled composites, and periodic porous polymer structures. Buckling instabilities in these non-homogeneous materials systems can exhibit remarkably complex morphologies. For example, the presence of the patterned array of nanoparticles in a polymer film resulted in two distinct critical strains for buckling, thus localizing the buckling to certain predetermined regions. In periodic porous polymer structures, buckling instabilities were shown to result in an interesting pattern transformation with a non-trivial morphology extending over a few thousand unit cells with almost no defects. These complex patterns were employed to create periodic functional nanomaterials which in turn exhibited unique optical properties. Furthermore, the pattern transformations induced by buckling instabilities were found to result in reversible changes in the photonic and phononic properties of these periodic structures and unusual negative Poisson's ratio.

There are numerous avenues such as flexible electronics and tunable surfaces where tremendous progress has been witnessed based on unique structural transformations associated with

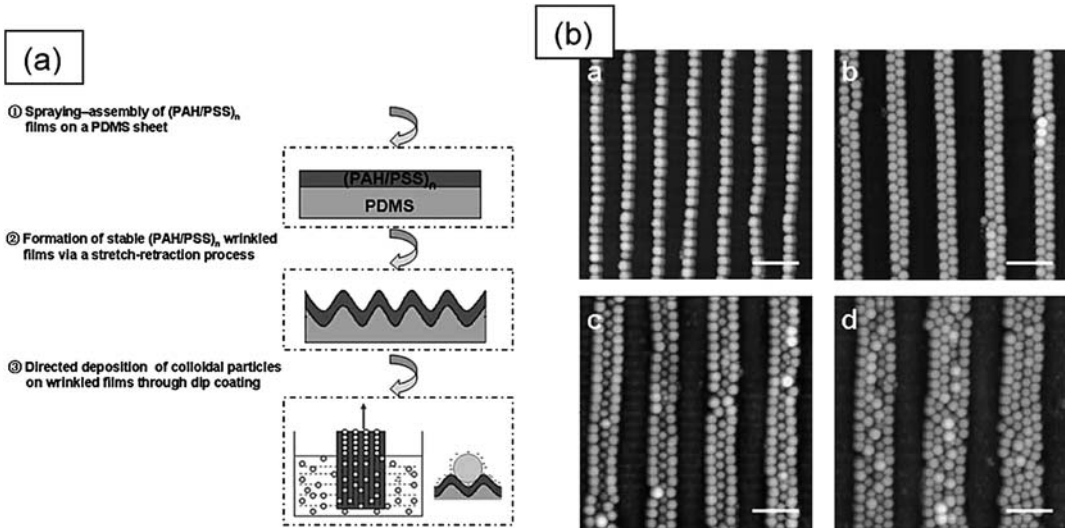

Fig. 10 (a) Schematic showing the patterning of the colloidal particles using the buckled surface as template. (b) AFM images of colloidal particle assemblies formed by process depicted in the schematic. Reprinted from ref. 23.

buckling instabilities. Considering the rapid progress, we envision that buckling-based patterning of nanomaterials and tunable photonic and phononic structures will play an important role in a number of emerging applications. Furthermore, buckling-based reversible changes in morphology present immense opportunity in biomedical applications, such as tissue engineering applications (2D and 3D porous, micro- and nano-fluidic channels) where the structure and microenvironment witnessed by the cells proliferating on the surface can be dynamically tuned.

Acknowledgements

The authors acknowledge S. Young for assistance with the manuscript and E. L. Thomas and M. Boyce for fruitful collaboration. This work of the authors in this field is supported

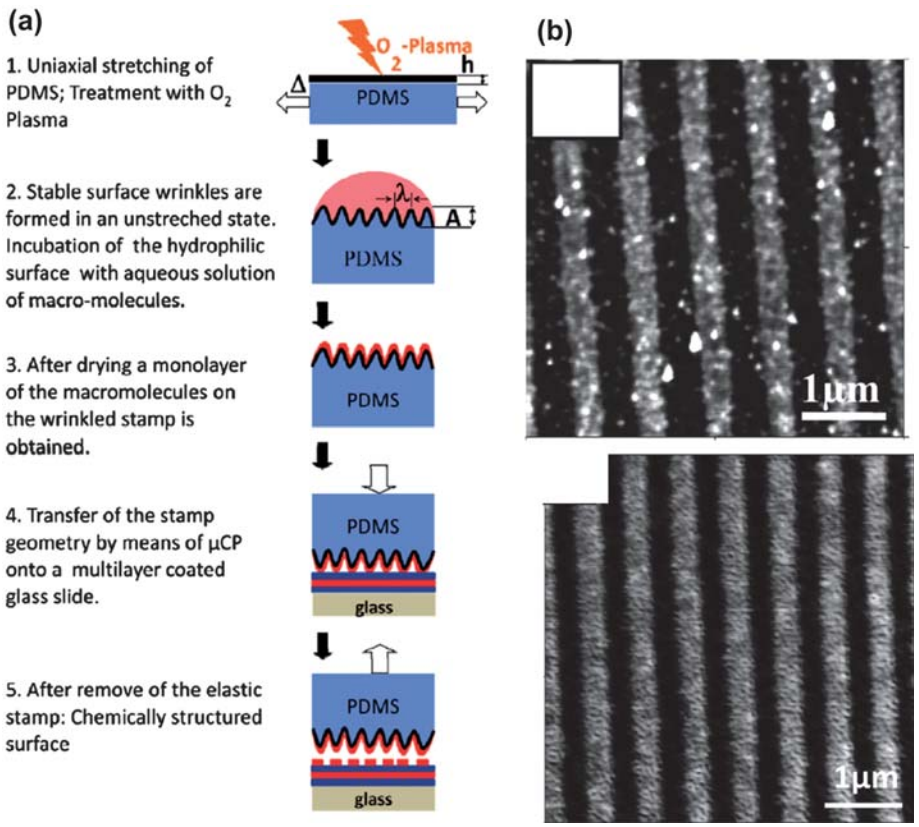

Fig. 11 (a) Schematic showing the patterning of the polyelectrolyte layers using buckles as surface relief structures. (b) AFM images of the patterned arrays of PEMs and BSA on PEI-terminated glass substrate. Reprinted from ref. 67.

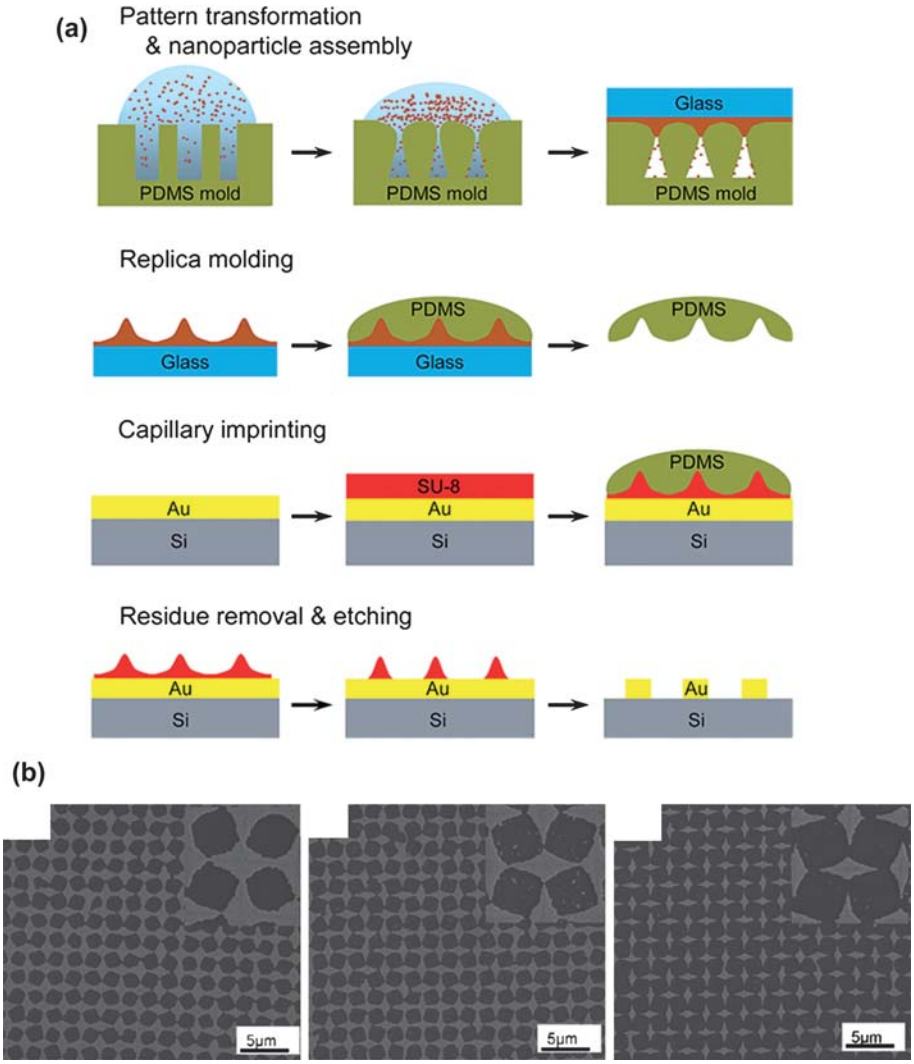

Fig. 12 (a) Schematic showing the patterning of nanoparticles and utilization of these patterns to create more complex structures using soft lithographic approach. (b) Series of SEM images showing the fine structure control attained by controlling the etching time of the resist. Reprinted from ref. 68.

by the National Science Foundation and Air Office of Scientific Research.

References

1 J. Genzer and J. Groenewold, *Soft Matter*, 2006, **2**, 310–323.
2 S. Timoshenko, *Theory of Plates and Shells*, McGraw-Hill, New York, 1940.
3 S. Timoshenko, *Theory of Elastic Stability*, McGraw-Hill, New York, 1988.
4 D. O. Bush and B. O. Almroth, *Buckling of Bars, Plates and Shells*, McGraw-Hill, New York, 1975.
5 L. D. Landau and E. M. Lifshitz, *Elasticity Theory*, Nauka, Moscow, 1965.
6 J. S. Sharp and R. A. L. Jones, *Phys. Rev. E: Stat, Nonlinear, Soft Matter Phys.*, 2002, **66**, 011801.
7 E. Cerda, K. Ravi-Chandar and L. Mahadevan, *Nature*, 2002, **419**, 579–598.
8 E. Cerda and L. Mahadevan, *Phys. Rev. Lett.*, 2003, **90**, 074302.
9 N. Bowden, S. Brittain, A. G. Evans, J. W. Hutchinson and G. M. Whitesides, *Nature*, 1998, **393**, 146–149.
10 M. W. Moon, H. M. Jensen, J. W. Hutchinson, K. H. Oh and A. G. Evans, *J. Mech. Phys. Solids*, 2002, **50**, 2355–2377.
11 K. Efimenko, M. Rackaitis, E. Manias, A. Vaziri, L. Mahadevan and J. Genzer, *Nat. Mater.*, 2005, **4**, 293–297.
12 L. Mahadevan and S. Rica, *Science*, 2005, **307**, 1740.
13 J. Hiller, J. D. Mendelsohn and M. F. Rubner, *Nat. Mater.*, 2002, **1**, 59–63.
14 J. Huang, M. Juszkiewicz, W. H. de Jeu, E. Cerda, T. Emrick, N. Menon and T. P. Russell, *Science*, 2007, **317**, 650–653.
15 J.-T. Chen, M. Zhang and T. P. Russell, *Nano Lett.*, 2007, **7**, 183–187.
16 Y. Sun, W. M. Choi, H. Jiang, Y. Y. Huang and J. A. Rogers, *Nat. Nanotechnol.*, 2006, **1**, 201–207.
17 J. Xiao, H. Jiang, D. Y. Khang, J. Wu, Y. Huang and J. A. Rogers, *J. Appl. Phys.*, 2008, **104**, 033543.
18 D.-Y. Khang, J. Xiao, C. Kocabas, S. MacLaren, T. Banks, H. Jiang, Y. Y. Huang and J. A. Rogers, *Nano Lett.*, 2008, **8**, 124–130.
19 E. P. Chan, E. J. Smith, R. C. Hayward and A. J. Crosby, *Adv. Mater.*, 2008, **20**, 711–716.
20 P. Lin, S. Vajpayee, A. Jagota, C.-H. Hui and S. Yang, *Soft Matter*, 2008, **4**, 1830–1835.
21 Y. Sun and J. A. Rogers, *J. Mater. Chem.*, 2007, **17**, 832–840.
22 J. A. Rogers, T. Someya and Y. Huang, *Science*, 2010, **327**, 1603–1607.
23 C. H. Lu, H. Mohwald and A. Fery, *Soft Matter*, 2007, **3**, 1530–1536.
24 P. J. Yoo, K. Y. Suh, S. Y. Park and H. H. Lee, *Adv. Mater.*, 2002, **14**, 1383–1387.

25 M.-W. Moon, S. H. Lee, J.-Y. Sun, K. H. Oh, A. Vaziri and J. W. Hutchinson, *Proc. Natl. Acad. Sci. U. S. A.*, 2007, **104**, 1130–1133.
26 Z. Y. Huang, W. Hong and Z. Suo, *Phys. Rev. E: Stat. Phys., Plasmas, Fluids, Relat. Interdiscip. Top.*, 2004, **70**, 030601.
27 J. Song, H. Jiang, Y. Huang and J. A. Rogers, *J. Vac. Sci. Technol., A*, 2009, **27**, 1107–1125.
28 C. M. Stafford, C. Harrison, K. L. Beers, A. Karim, E. J. Amis, M. R. Vanlandingham, H. C. Kim, W. Volksen, R. D. Miller and E. E. Simonyi, *Nat. Mater.*, 2004, **3**, 545–550.
29 C. Jiang, X. Wang, R. Gunawidjaja, Y.-H. Lin, M. K. Gupta, D. L. Kaplan, R. R. Naik and V. V. Tsukruk, *Adv. Funct. Mater.*, 2007, **17**, 2229–2237.
30 S. Singamaneni, M. E. McConney and V. V. Tsukruk, *Adv. Mater.*, 2010, **22**, 1263–1268.
31 S. Singamaneni, M. E. McConney and V. V. Tsukruk, *ACS Nano*, 2010, **4**, 2327–2337.
32 A. J. Nolte, R. E. Cohen and M. F. Rubner, *Macromolecules*, 2006, **39**, 4841–4847.
33 C. Lu, I. Dönch, M. Nolte and A. Fery, *Chem. Mater.*, 2006, **18**, 6204–6210.
34 C. Jiang, S. Singamaneni, E. Merrick and V. V. Tsukruk, *Nano Lett.*, 2006, **6**, 2254–2259.
35 Y. H. Lin, C. Jiang, J. Xu, Z. Lin and V. V. Tsukruk, *Adv. Mater.*, 2007, **19**, 3827–3832.
36 C. Jiang, S. Markutsya, Y. Pikus and V. V. Tsukruk, *Nat. Mater.*, 2004, **3**, 721–728.
37 C. Jiang, S. Markutsya, H. Shulha and V. V. Tsukruk, *Adv. Mater.*, 2005, **17**, 1669–1673.
38 C. Jiang, M. E. McConney, S. Singamaneni, E. Merrick, Y. Chen, J. Zhao, L. Zhang and V. V. Tsukruk, *Chem. Mater.*, 2006, **18**, 2632–2634.
39 D. P. Holmes and A. J. Crosby, *Adv. Mater.*, 2007, **19**, 3589–3593.
40 M. R. Begley, M. Utz and U. Komaragiri, *J. Mech. Phys. Solids*, 2005, **53**, 2119–2140.
41 M. Utz and M. R. Begley, *J. Mech. Phys. Solids*, 2008, **56**, 801–814.
42 S. Singamaneni, M. C. LeMieux, H. P. Lang, Ch. Gerber, Y. Lam, S. Zauscher, P. G. Datskos, N. V. Lavrik, H. Jiang, R. R. Naik, T. J. Bunning and V. V. Tsukruk, *Adv. Mater.*, 2008, **20**, 653–680.
43 M. E. McConney, K. D. Anderson, L. L. Brott, R. R. Naik and V. V. Tsukruk, *Adv. Funct. Mater.*, 2009, **19**, 2527–2544.
44 R. Gunawidjaja, C. Jiang, H. Ko and V. V. Tsukruk, *Adv. Mater.*, 2006, **18**, 2895–2899.
45 R. Gunawidjaja, C. Jiang, S. Peleshanko, M. Ornatska, S. Singamaneni and V. V. Tsukruk, *Adv. Funct. Mater.*, 2006, **16**, 2024–2034.
46 R. Gunawidjaja, H. Ko, C. Jiang and V. V. Tsukruk, *Chem. Mater.*, 2007, **19**, 2007–2015.
47 T. R. Hendricks and I. Lee, *Nano Lett.*, 2007, **7**, 372–379.
48 J. Smith, J. Hodgins, I. Oppenheim and A. Witkin, *ACM Trans. Graph.*, 2002, **21**, 295–301.
49 J. H. Jang, C. K. Ullal, T. Y. Choi, M. C. Lemieux, V. V. Tsukruk and E. L. Thomas, *Adv. Mater.*, 2006, **18**, 2123–2127.
50 J. H. Jang, S. J. Jhaveri, B. Rasin, C. Koh, C. K. Ober and E. L. Thomas, *Nano Lett.*, 2008, **8**, 1456–1460.
51 S. Singamaneni, S. Chang, J.-H. Jang, W. Davis, E. L. Thomas and V. V. Tsukruk, *Phys. Chem. Chem. Phys.*, 2008, **10**, 4093–4105.
52 S. Singamaneni, E. Kharlampieva, M. E. McConney, H. Jiang, J.-H. Jang, E. L. Thomas, T. J. Bunning and V. V. Tsukruk, *Adv. Mater.*, 2010, **22**, 1369–1373.
53 V. S. Deshpande, M. F. Ashby and N. A. Fleck, *Acta Mater.*, 2001, **49**, 1035–1040.
54 T. Mullin, S. Deschanel, K. Bertoldi and M. C. Boyce, *Phys. Rev. Lett.*, 2007, **99**, 084301.
55 N. Triantafyllidis, M. D. Nestorovic and M. W. Schraad, *J. Appl. Mech.*, 2006, **73**, 505–515.
56 K. Bertoldi and M. C. Boyce, *Phys. Rev. B: Condens. Matter*, 2008, **77**, 052105.
57 K. Bertoldi, P. M. Reis, S. Willshaw and T. Mullin, *Adv. Mater.*, 2010, **22**, 361–366.
58 Y. Zhang, E. A. Matsumoto, A. Peter, P. Lin, R. D. Kamien and S. Yang, *Nano Lett.*, 2008, **8**, 1192–1196.
59 S. Singamaneni, K. Bertoldi, S. Chang, J.-H. Jang, E. L. Thomas, M. Boyce and V. V. Tsukruk, *ACS Appl. Mater. Interfaces*, 2009, **1**, 42–47.
60 S. Singamaneni, K. Bertoldi, S. Chang, J.-H. Jang, S. Young, E. L. Thomas, M. Boyce and V. V. Tsukruk, *Adv. Funct. Mater.*, 2009, **19**, 1426–1436.
61 J. H. Jang, C. Y. Koh, K. Bertoldi, M. C. Boyce and E. L. Thomas, *Nano Lett.*, 2009, **9**, 2113–2119.
62 A. L. Volynskii, S. Bazhenov, O. V. Lebedeva and N. F. Bakeev, *J. Mater. Sci.*, 2000, **35**, 547–554.
63 C. Lu, H. Möhwald and A. Fery, *Chem. Mater.*, 2008, **20**, 7052–7059.
64 K. Y. Suh, Y. S. Kim and H. H. Lee, *Adv. Mater.*, 2001, **13**, 1386–1389.
65 H. Ko, C. Jiang and V. V. Tsukruk, *Chem. Mater.*, 2005, **17**, 5489–5497.
66 X. Zhu, Y. Zhang, D. Chandra, S.-C. Cheng, J. M. Kikkawa and S. Yang, *Appl. Phys. Lett.*, 2008, **93**, 161911.
67 M. Pretzl, A. Schweikart, C. Hanske, A. Chiche, U. Zettl, A. Horn, A. Boker and A. Fery, *Langmuir*, 2008, **24**, 12748–12753.
68 Y. Zhang, J. C. Reed and S. Yang, *ACS Nano*, 2009, **3**, 2412–2418.

